X-ray-scattering study of higher harmonic satellites near the antiferromagnetic phase transitions in rare-earth metals

G. Helgesen
Brookhaven National Laboratory, Upton, New York 11973
and Institute for Energy Technology, N-2007 Kjeller, Norway

J. P. Hill, T. R. Thurston, and Doon Gibbs
Brookhaven National Laboratory, Upton, New York 11973
(Received 15 May 1995)

We present resonant x-ray magnetic scattering studies of the temperature dependence of the magnetic order parameters of Dy, Ho, Er, and Tm single crystals near their antiferromagnetic phase transitions. The experimentally determined values of the critical exponent β of Er and Tm, which have c-axis modulated structures, are nearly equal and consistent with the mean-field value ($\beta=0.47\pm0.05$ and $\beta=0.49\pm0.06$, respectively). The measured values of Dy and Ho, which have spiral magnetic structures, are lower ($\beta=0.36\pm0.04$ and $\beta=0.41\pm0.04$, respectively). In addition to the primary magnetic order parameters, we have measured the temperature dependence of the intensities of up to four higher harmonics. The exponents of the higher harmonic satellites of Er and Tm exhibit mean-field-like scaling, while those of Ho do not. We discuss these results within the context of simple corrections to mean-field scaling, based on the three-dimensional XY model. We also report measurements of the temperature dependence of the c-axis lattice constants and magnetic wave vectors of all four metals. It is found that the magnetic correlation lengths are reduced near transitions to ferrimagnetic and ferromagnetic phases.

I. INTRODUCTION

The magnetic structures of the heavy rare-earth metals, observed near their Néel temperatures T_N, are among the simplest incommensurate antiferromagnets known. Dy and Ho have basal-plane, spiral structures, while Er and Tm have c-axis modulated (CAM) structures.[1,2] The occurrence of the magnetic structures generally reflects the balance among single-ion crystal-field interactions, which are characteristic of the hexagonally closed packed lattice, and the two-ion exchange interaction, which is mediated by the conduction electrons.[3] Below T_N, the temperature dependence of the exchange and crystal-field interactions, in addition to that of the accompanying magnetoelastic interactions, modify the balance, and in some cases lead to incommensurate-commensurate transformations. Many qualitative features of the magnetic phase behavior of rare-earth metals are well understood, and have been successfully modeled using mean-field theory.[3]

Despite this progress, the magnetic critical behavior exhibited by the rare-earth metals is unresolved. The antiferromagnetic phase transitions near T_N are generally believed to be continuous,[4–6] although hysteresis and other indications of weakly first-order behavior have been reported in some experiments on Ho (Refs. 7 and 8) and Dy.[9] There are at least two proposed universality classes for the spiral rare earths: Bak and Mukamel[10] have suggested a symmetric $O(n)$ model with $n=4$, whereas Kawamura[11] has proposed a chiral universality class. Barak and Walker[12] have proposed that the transformation is driven first order by fluctuations, and Azaria, Delmotte, and Jolicover[13] that the critical behavior is controlled by tricritical points in the phase diagram. Fewer theoretical studies have been made of the nature of the antiferromagnetic transition in the CAM materials. Both the three-dimensional (3D) XY and mean-field universality classes have been proposed for Er.[5]

The set of critical exponents (β,γ,ν) as determined by neutron-scattering measurements is shown in Table I. The exponents predicted by the $O(n=4)$,[10] chiral,[11] and 3D XY models[14] are $(\beta,\gamma,\nu)=(0.39,1.39,0.70)$, $(0.25,1.10,0.53)$, and $(0.35,1.32,0.67)$, respectively. As may be seen, none of the proposed models satisfactorily accounts for all of the measured exponents. Complicating matters further, there are discrepancies among the experimental values, for example, for β of the staggered magnetization of erbium. More recently, high-resolution x-ray- and neutron-scattering studies of the magnetic correlations have revealed evidence of a second length scale near T_N in a variety of materials including Ho, Tb, NpAs, and others.[15–17] The origin of this additional scattering is not understood, although it is believed to be related to the presence of random strain fields near the surface.

In this paper, we present high-resolution, resonant x-ray magnetic scattering studies of the temperature dependence of the magnetic order parameter at the antiferromagnetic ordering transitions of bulk Dy, Ho, Er, and Tm single crystals. A motivation for the application of x-ray-scattering techniques in these experiments is the largely extinction-free character of the x-ray magnetic cross section, in contrast to neutron diffraction, where extinction has complicated measurements of the exponent

TABLE I. Some parameters for the rare earths studied in this experiment and values of their critical exponents reported in the literature.

Sample	Dy	Ho	Er	Tm
Dimensions/mm^3	8×2.5×2.5	9×4×4	9×4×3	4.3×7×3.6
Crystal mosaic	<0.08°	<0.014°	<0.04°	<0.07°
L_{III} energy/eV	7790	8072(E1) 8064(E2)	8358	8648
T_N/K	180.6	131.4	87.7	56.0
a/Å (300 K)	3.590	3.577	3.559	3.538
c/Å (T_N)	5.645	5.603	5.562	5.515
τ/c^* (T_N)	0.243	0.279	0.283	0.271
β (theory)	0.39,[a] 0.25[b]		0.35[c]	
β (earlier expt.)	0.335±0.01[d] 0.39±0.04[h]	0.39[e]	0.35±0.03[f] 0.39[i] 0.48±0.02[c]	0.25–0.30[g] 0.37±0.03[f]
β (this expt.)	0.36±0.04	0.41±0.04	0.47±0.05	0.49±0.06
γ	1.05±0.07[j]	1.14±0.10[j] 1.24±0.15[k]	0.73±0.06[f] 0.96±0.06[c]	0.90±0.04[f]
ν	0.57±0.05[j]	0.57±0.04[j] 0.54±0.04[k]	0.41±0.04[f] 0.49±0.02[c]	0.43±0.02[f]

[a]Reference 10.
[b]Reference 11.
[c]Reference 5.
[d]Reference 35.
[e]Reference 36.
[f]Reference 6.
[g]Reference 21.
[h]Reference 34.
[i]Reference 37.
[j]Reference 4.
[k]Reference 15.

β. Another important feature of the x-ray-scattering results is the characterization of the temperature dependence of up to four higher harmonic satellites, in addition to that of the primary order parameter. For the spiral rare earths, these harmonics are resonant in origin, arising from the dipole and quadrupole allowed transitions near the L_{III} absorption edge.[18,19] They are a unique property of the x-ray cross section. For the CAM structures, the higher *even* harmonics originate in the charge scattering arising from lattice modulations,[20,21] and have escaped detection by neutron scattering. It has been shown previously that for some systems with incommensurate wave vectors these higher harmonics represent secondary order parameters, which are related to the primary order parameters via crossover exponents.[22] The identification of such crossover exponents for the rare earths may facilitate identification of their universality classes.

Briefly, we have found that the exponents β for the order parameters of Dy and Ho are approximately equal to within the error bars, with values 0.36±0.04 and 0.41±0.04, respectively. The temperature dependence of the higher resonant harmonics of Dy and Ho also exhibits power-law behavior, but their exponents are inconsistent with mean-field scaling (that is, the exponent for the nth harmonic $\beta_n \neq n\beta$). In contrast, the exponents β found for Er and Tm are consistent with the mean-field value, $\beta=0.47\pm0.05$ and $\beta=0.49\pm0.06$, respectively. Further, the second- and fourth-order charge scattering harmonics exhibit mean-field scaling. In addition, we present results of comprehensive, high-resolution studies of the temperature dependence of the magnetic wave vectors and c-axis lattice constants obtained for all four materials in their antiferromagnetically ordered phases. For the most part, these results are consistent with the results of earlier studies, including the observations of lock-in transformations, etc. However, other trends emerge when these results are plotted versus T/T_N, and compared.

The details of our experiments are described in Sec. II. Our results and a discussion are presented in Sec. III. We summarize in Sec. IV.

II. THE EXPERIMENT

Our x-ray-scattering experiments were performed on the bending magnet beam line X22C and the wiggler beam line X25 at the National Synchrotron Light Source. X22C and X25 are doubly focused beam lines with double-crystal Ge(111) and Si(111) monochromators, respectively. Both were equipped with Ge(111) analyzing crystals. In this configuration, X22C delivers approximately 10^{11} photons/sec at 8 keV photon energy with about 5–10 eV energy resolution in a $\sim$1 mm^2 spot at the sample. The flux at X25 is approximately ten times greater. The intensities of the incident and scattered beams were monitored using NaI scintillation counters. A typical experimental resolution obtained near the primary magnetic satellite at momentum transfer $Q=1.8$ Å^{-1} was 7×10^{-4} Å, 4×10^{-4}, and 2×10^{-2} Å^{-1} full width at half maximum (FWHM) in the longitudinal, transverse, and out-of-scattering plane directions, respec-

tively. All of the x-ray magnetic scattering experiments were performed at the L_{III} absorption edges of the respective rare-earth metals. These are 7790, 8072, 8358, and 8648 eV for Dy, Ho, Er, and Tm, respectively. Typical x-ray penetration depths at these energies are about 0.5 μm. All of the rare-earth samples were obtained from the Materials Preparation Center at Ames Laboratory. Their surfaces were mechanically polished and chemically etched in a passivating solution, as has been described elsewhere.[23] The sample mosaics obtained at the (0,0,2) reflections are all excellent, and listed in Table I. The samples were mounted inside closed-cycle He refrigerators and the temperature monitored using Si-diode thermometers.

The crystal structures of all of the elements in the second half of the lanthanide series are hexagonally closed packed. However, the competition among single-ion crystal-field interactions and two-ion exchange interactions, together with the magnetoelastic coupling which accompanies magnetic ordering, give rise to a variety of distinct magnetic structures. Just below T_N, the result is a magnetic spiral structure along the c axis in the elements Dy and Ho and a sinusoidally modulated, c-axis magnetic structure in Er and Tm. At lower temperatures, the increasing importance of the hexagonal anisotropy leads to first-order transformations in all of the rare earths, e.g., to a planar ferromagnetic structure in Dy, to a commensurate CAM ferrimagnet in Tm, and to sequences of lock-in transformations to various commensurate structures in Ho and Er. The details of these structures and of their commensurate-incommensurate transformations have been the subject of numerous earlier neutron- and x-ray-scattering studies.[2,3]

The diffraction patterns of the metals studied in this paper consist of pairs of magnetic satellites split symmetrically along the c axis about each of the chemically allowed charge scattering Bragg peaks. The splitting of the magnetic peaks relative to the charge peaks corresponds to the magnetic wave vector τ, which is inversely proportional to the wavelength of the ordered magnetic structure. It has been shown earlier that the magnetic cross section is resonantly enhanced when the incident x-ray energy is tuned near an L_{III} edge, with increases in the measured intensity as great as a factor 50.[18,19] X-ray resonant magnetic scattering has been described on the basis of electric dipole and quadrupole transitions between $2p$ core states and the $5d$ and $4f$ valence levels, respectively.[24] Specifically, the incident photon promotes a core electron to an unoccupied, symmetry-allowed valence state, which subsequently decays. The photon emitted in this decay corresponds to the elastic, magnetic scattering. For the particular case of a magnetic spiral, first- and second-order harmonics occur at the dipole resonance, and are located in reciprocal space along the c^* axis at positions $Q/c^*=2m\pm\tau$ and $2m\pm2\tau$ ($m=1,2,\ldots$ and $c^*=2\pi/c\approx1.13$ Å^{-1}), respectively.[18] For quadrupole excitations, which occur at a slightly lower incident x-ray energy, there are four resonant harmonics at $Q/c^*=2m\pm n\tau$, where $n=1$, 2, 3, or 4. The detailed energy and polarization dependence of these processes is well understood in rare-earth metals.[19,21,24–27] Similar resonant magnetic, higher order harmonics have not been observed for the CAM structures. More easily observed in Er and Tm are lattice modulations which produce second- and fourth-order charge scattering satellites along the c axis. Charge scattering harmonics of even order are not allowed along the c axis in spiral structures, and have not been observed in Ho or in Dy.

III. RESULTS AND DISCUSSION

A. Order parameter and higher harmonics

Figure 1 shows scans obtained at the L_{III} edge of Er taken in the CAM phase along the $(0,0,L)$ direction through $L=2+\tau$, $2+2\tau$, $2+3\tau$, and $2+4\tau$. τ is the magnetic wave vector in c^* units. There is a difference in intensity of about two orders of magnitude between the magnetic satellites of first and third order. A similar ratio was found between the intensities of the second- and

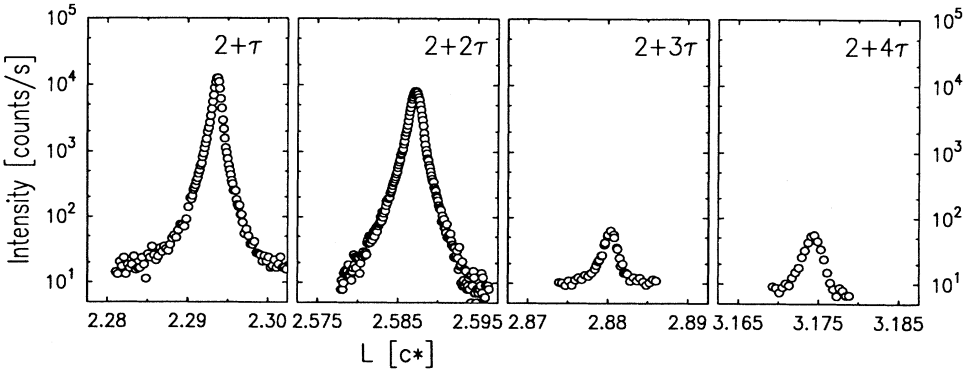

FIG. 1. Scans taken along the $(0,0,L)$ direction for Er at $T=60$ K. The peaks are located at $Q=(2+n\tau)c^*$ with $n=1$, 2, 3, and 4. Here, $c^*=1.13$ Å^{-1} and the magnetic wave vector $\tau=0.292$. All scans were taken at the L_{III} absorption edge of Er.

fourth-order satellites which arise from charge scattering. The integrated intensities calculated from longitudinal (similar to those shown in Fig. 1) and transverse scans of the primary and higher order harmonics exhibited by Dy, Ho, Er, and Tm are shown on a logarithmic scale versus temperature in Fig. 2. The temperature scales have been normalized by the respective Néel temperatures T_N (see Table I). In each case, the scattering from the first harmonic corresponds to the magnetic scattering obtained at the dipole resonance of the respective L_{III} absorption edge. In this regard, it should be noted that the dominant contribution to the cross section arises from a two-spin correlation function analogous to neutron diffraction.[27–29] The second- and third-order harmonics exhibited by Ho are resonant harmonics arising from the dipole and quadrupole excitations, respectively. The latter were obtained at a slightly lower energy ($E=8064$ eV) than the former, but are believed to have a temperature dependence which predominantly mirrors that of the dipole excitations near T_N.[30] The data for Ho have been discussed previously.[31]

The second and fourth-order harmonics exhibited by erbium and thulium correspond to charge scattering arising from lattice modulations.[20,21,32] It is important to note that the temperature dependence of the second- and fourth-order harmonics observed for both Er and Tm was also obtained at incident x-ray energies removed from their respective L_{III} edges. No differences were found when compared to the data obtained at resonance. In our opinion, the third-order harmonic for erbium is a structural harmonic of the first, corresponding to a distortion of the c-axis magnetic modulation from perfectly sinusoidal behavior. A similar third harmonic has been observed by neutron diffraction, reduced by three to four orders of magnitude in intensity.[5,33] It is also possible that this scattering could arise from the quadrupole resonance, although we believe that contribution would be very small and should take its maximum at a slightly lower energy.

We first discuss the temperature dependence of the integrated intensity of the primary harmonic, which is shown for all four crystals on a log-log plot in Fig. 3. The best fits of the intensities to a power law, $I_\tau(t) \propto t^{2\beta}$, in the interval 10^{-3}–0.2 of the reduced temperature $t=(T_N-T)/T_N$, are shown by solid lines. The fitted exponents are summarized in Table I. All the exponents were calculated from more data sets than are shown in Fig. 2. Minor differences among the transition temperatures T_N and the critical exponents β were found when data from different runs on a sample were analyzed. The best-fit values of β given below represent averages of the results taken for at least two decades in t. The error bars represent the maximum variation which was found when allowing also for an uncertainty of about ± 0.05 K in the value of T_N.

Our best-fit value for the exponent β of Dy, $\beta=0.36\pm0.04$, agrees to within the error bars with the value $\beta=0.39\pm0.04$ measured in neutron-scattering experiments by du Plessis, van Doorn, and van Delden,[34] and with $\beta=0.335$ found by Loh, Chien, and Walker[35] from Mössbauer techniques. The value $\beta=0.41\pm0.04$ found for Ho, which has the same magnetic structure as Dy, appears slightly larger than the value found for Dy, but agrees comfortably to within the error bars. It is also consistent with the value found in earlier neutron-scattering measurements.[36] Both of our measured exponents are significantly higher than the value $\beta=0.25$ predicted for the chiral universality class,[11] but agree with the value $\beta=0.39$ predicted by Bak and Mukamel for the O(4) model.[10] The prediction of the 3D XY model $\beta=0.345$ (Ref. 14) lies within the experimental range determined for Dy, but outside that for Ho. Unfortunately, it is difficult to characterize exponents with accuracy better than $\pm 10\%$.

The values of the critical exponent β of Er and Tm are nearly the same, $\beta=0.47\pm0.05$ for Er and $\beta=0.49\pm0.06$ for Tm, and are equal to the mean-field value $\beta=0.5$ to within the error bars. Our value of β for Er is higher

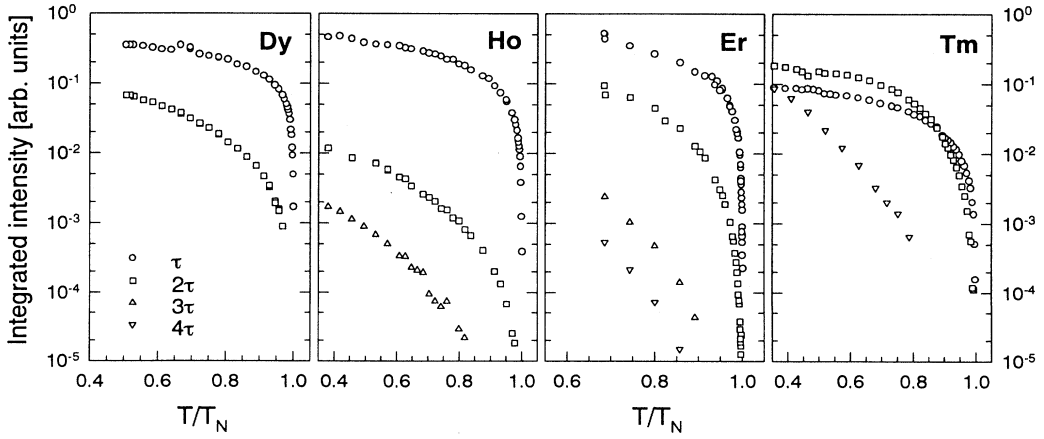

FIG. 2. Integrated intensity of the $(0,0,2-n\tau)$ satellites of Dy, Ho, and Tm and the $(0,0,2+n\tau)$ satellites of Er ($n=1$–4), measured at their respective L_{III} edges. See text for discussion.

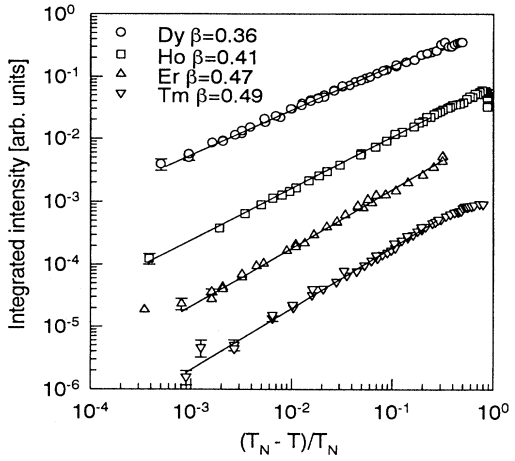

FIG. 3. Integrated intensity of the $(0,0,2-\tau)$ magnetic satellite of Dy, Ho, and Tm, and the $(0,0,2+\tau)$ satellite of Er on log-log plots as a function of the reduced temperature. The best fits to power-law behavior are shown as solid lines.

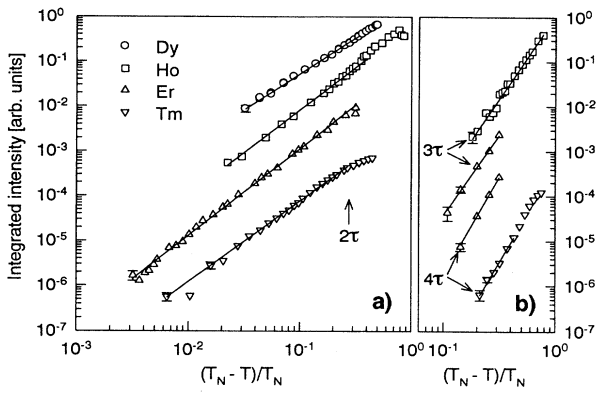

FIG. 4. Integrated intensity vs temperature of the higher harmonic satellites. The solid lines show the best fits to power-law behavior $I_{n\tau} \propto (T_N - T)^{2\beta_n}$. (a) Second harmonics with exponents $\beta_2 = 0.80$, 0.95, 0.97, and 0.90 for Dy, Ho, Er, and Tm, respectively. (b) The curves (from top to bottom) show the third harmonic of Ho, the third and fourth harmonics of Er, and the fourth harmonic of Tm. Their exponents are $\beta_3(\text{Ho}) = 1.85$, $\beta_3(\text{Er}) = 1.8$, $\beta_4(\text{Er}) = 2.2$, and $\beta_4(\text{Tm}) = 2.1$.

than that reported by Hagen *et al.*[6] ($\beta = 0.35$), but is in good agreement with recent neutron-scattering measurements by Lin, Collins, and Holden[5] ($\beta = 0.48 \pm 0.02$). Crossover behavior from mean-field exponents away from T_N to $\beta = 0.39$ near T_N has been reported previously for Er,[37] but was not observed in the present studies. Several different values of β have also been reported for Tm (see Table I). The value $\beta = 0.49$ found in our x-ray-scattering experiment is in good agreement with the value we found for Er, which has a similar magnetic structure, but is larger than earlier published values.[6]

We turn now to a discussion of the temperature dependence of the higher harmonics of the rare earths. Near T_N, the integrated intensities of the higher harmonics shown in Fig. 2 decrease much faster than their respective primaries. The intensity vs temperature of the second-order satellites is shown in a double-logarithmic plot in Fig. 4(a) and the third and fourth harmonics are shown in Fig. 4(b). As can be seen in Fig. 4, the integrated intensities of the higher harmonics show power-law behavior as functions of the reduced temperature. However, due to the weakness of the higher harmonics for temperatures close to T_N, we were unable to find reliable values of T_N from these curves. The Néel temperatures were therefore fixed at the values found from the primary magnetic satellites and only the exponents β_n were fitted.

Higher order satellites, which represent secondary order parameters,[22] have previously been measured by neutron scattering in experiments on Er (Ref. 33) and in structural phase transitions.[38] The temperature dependence of incommensurate higher order satellites reflects the crossover exponents due to the respective symmetry-breaking perturbations in the Hamiltonian of the spin system. The order parameter exponents β_n are related to the primary critical exponents of the particular model system via $\beta_n = 2 - \alpha - \phi_n$, where α is the specific-heat exponent and ϕ_n is a crossover exponent. For example, for the 3D XY model, the exponent ϕ_2 (or equivalently β_2) measures the crossover caused by perturbations of uniaxial anisotropy, and ϕ_3 (or β_3) may be associated with perturbations having the symmetry of the three-state Potts model. A clear demonstration of the significance of secondary order parameters at a continuous phase transformation was presented in an x-ray-scattering study of liquid crystal films by Brock *et al.*[39] In their experiments, up to nine Fourier components C_{6n} of the hexatic order present in the liquid crystal films were resolved. These secondary order parameters were related to the primary order parameter C_6 via $C_{6n} = (C_6)^{\sigma_n}$. For the XY model, the theory[40,41] predicts that the effective exponents $\sigma_n = \beta_n / \beta_1$ should have the form

$$\sigma_n = n + \lambda n(n-1) , \tag{1}$$

where n is the order of the harmonic and λ is a temperature-independent parameter which depends only weakly on n. Brock *et al.*[39] deduced a value $\lambda \approx 0.3$ for the 3D XY model describing their liquid crystal data in excellent agreement with theoretical calculations.[40]

In our earlier studies of Ho,[31] we found that the best-fit exponents obtained for the higher order satellites of Ho do not appear to exhibit mean-field scaling, that is, $\beta_n \neq n\beta$. Specifically, we reported that $\beta = 0.41 \pm 0.04$, $\beta_2 = 0.95 \pm 0.10$, and $\beta_3 = 1.85 \pm 0.10$ for Ho. In order to analyze the scaling of the higher harmonics, we used a scaling assumption similar to that employed in Ref. 39, namely, that the intensity of the nth order harmonic

$$I_{n\tau}(t) \propto [I_\tau(t)]^{\sigma_n} , \tag{2}$$

at a reduced temperature t. It was found that the value of σ_n for $n = 2$ and 3 showed an n dependence similar to

Eq. (1) with the best-fit value of the parameter λ given by $\lambda=0.22\pm0.08$.[31] However, the assumption that Eq. (1) for the scaling of the higher harmonics may be applied to spiral antiferromagnets, for which the universality class is still unclear, has not been proven.

For the magnetic, second-order satellite of Dy shown in Fig. 4(a), we find that $\beta_2=0.80\pm0.10$ [shown by a solid line in Fig. 4(a)]. The similarity of the magnetic structures near T_N of Dy and Ho suggests that they belong to the same universality class and show similar scaling behavior. Since the error bars of the fitted exponents for Dy are large, $1.8<\beta_2/\beta<2.8$, we are unable to rule out a mean-field-like scaling of the exponents β_n. One should note, however, that the values of both exponents β and β_2 are smaller than their mean-field values. By applying Eqs. (1) and (2), it was observed that the value of λ found for Ho also gave reasonably good scaling of I_τ and $I_{2\tau}$ for Dy. However, since the temperature dependence of a possible third-order satellite of Dy was not studied in these experiments, we are unable to draw clear conclusions about the scaling of the harmonics in Dy.

The best-fit values for the exponents of the higher order satellites of the c-axis modulated rare earths are $\beta_2=0.97\pm0.10$, $\beta_3=1.8\pm0.3$, and $\beta_4=2.2\pm0.3$ for Er and $\beta_2=0.90\pm0.15$, $\beta_4=2.1\pm0.3$ for Tm.[42] Since the mean-field values $\beta_n=n/2$ fall well within the error bars of our measured exponents, these results support the suggestion of Lin, Collins, and Holden[5] that Er exhibits mean-field behavior. Our results indicate that this is also the case for Tm. This conclusion differs from that of another recent neutron-scattering study[6] which supported a 3D XY universality class for both Er and Tm.

A mean-field-like scaling of the higher order exponents β_n as was suggested by the best-fit values found for Er and Tm corresponds to $\lambda=0$ in Eq. (1). Unfortunately, attempts to extract a statistically significant value of λ directly from our data on Er and Tm using Eqs. (1) and (2) were unsuccessful, which reflects the limited data available near T_N. Nevertheless, we believe that these first scaling results for higher harmonics of rare earths are interesting and hope that they may provide motivation for more work on this problem, especially, experiments at more intense synchrotron sources.

B. c-axis lattice constants and magnetic wave vectors

The temperature dependence of the c-axis lattice constants and magnetic wave vectors of each of the samples studied in this work is plotted versus the normalized temperature T/T_N in Fig. 5. These parameters were determined at each temperature from measurements of the (0,0,2), (0,0,4), and (0,0,2$-\tau$) Bragg peak positions. The lattice constants c have also been normalized in each case by their values at T_N, $c(T_N)$ (see Table I). As is well known,[8,33,43] there are clear correlations between the temperature evolution of the c-axis lattice constants, which reflects the strain, and the magnetic wave vectors. These are particularly pronounced at the first-order transformations of the magnetic structure.

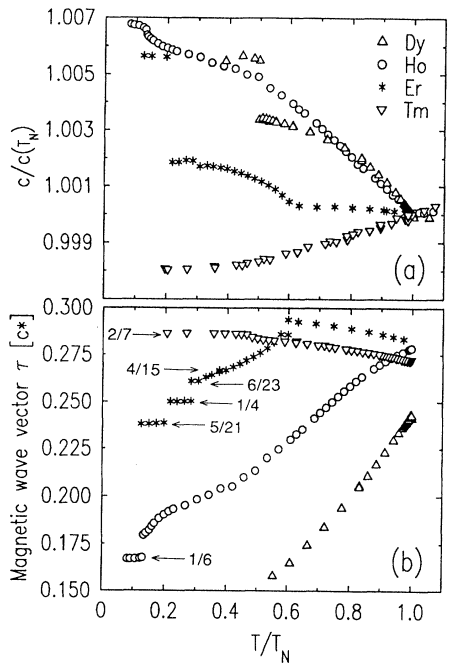

FIG. 5. (a) Lattice constant c versus temperature T for Dy, Ho, Er, and Tm. T and c are normalized by the Néel temperatures T_N and the lattice constants at T_N, $c(T_N)$, respectively (which can be found in Table I). (b) Magnetic wave vector τ (in c^* units) versus temperature.

On cooling below T_N, the relative expansion of the c-axis lattice constant is largest for Dy and Ho, little changed for Er, and negative for Tm. At $T=0.55T_N$, Dy undergoes a first-order transformation to a ferromagnetically ordered state, which is accompanied by a large jump in c ($\Delta c/c\approx2\times10^{-3}$). In Ho, the temperature dependence of the c-axis lattice constant changes slope at about $0.5T_N$ and jumps discontinuously at $0.13T_N$ (≈17 K). The latter corresponds to a lock-in transformation to a ferromagnetic cone structure with magnetic wave vector equal to $(\frac{1}{6})c^*$. Below $T=0.6T_N$, the c-axis lattice constant of Er starts to increase smoothly, but apparently nonlinearly, and then exhibits discontinuous jumps at about 0.28 and $0.20T_N$ (52, 25, and 17 K, respectively). The behavior at $0.6T_N$ corresponds to the transformation from a CAM structure to a cycloidal structure,[44] possessing both c-axis and basal-plane antiferromagnetic components. It is accompanied by a lock-in transformation to the wave vector $(\frac{2}{7})c^*$. The two discontinuities at lower temperatures correspond to lock-in transformations to wave vectors $(\frac{1}{4})c^*$ and $(\frac{5}{21})c^*$ as can be seen in Fig. 5(b). In contrast to the behavior of Dy, Ho, and Er, the c-axis lattice constant of Tm apparently decreases smoothly with decreasing temperature.

By correcting the measured lattice constants $c(T)$ below T_N for the normal thermal expansion [assumed to be constant and equal to the expansion coefficient k above T_N (Refs. 43 and 45)], we have estimated the change in lattice constant $\Delta c=c(T)-c(T_N)+k(T_N-T)$ due to magnetic ordering. Figure 6 shows the relative changes of lattice constant $\Delta c/c(T_N)$ plotted vs the intensity

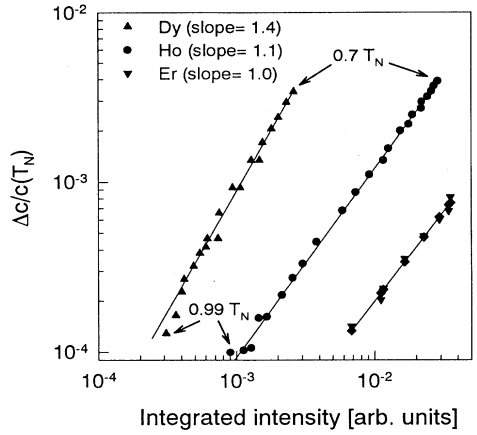

FIG. 6. The magnetic contribution to the change in lattice constant, Δc, vs the integrated intensity I_τ of the primary magnetic peak, as discussed in the text. The best fits of Δc to a power law of I_τ are shown as straight lines.

$I_\tau(T)$ of the primary magnetic peak in a double logarithmic plot. The figure contains data for the temperature range $0.7-0.99T_N$, corresponding to the helical phases of Dy and Ho and the CAM phase of Er. For Dy, we find $\Delta c \sim (I_\tau)^{1.4\pm0.15} \sim M^{2.8\pm0.3}$, since the integrated intensity $I_\tau \sim M^2$, where M is the sublattice magnetization. Similar estimates give $\Delta c \sim M^{2.2\pm0.3}$ for Ho and $M^{2.0\pm0.2}$ for Er. These results are qualitatively consistent with the simplest theory, in which the magnetoelastic contributions to the free energy are linear in the strain and the elastic contributions are quadratic. Since the coefficients of the magnetoelastic terms are even functions of the magnetization,[3] minimizing the free energy leads to a quadratic dependence of Δc on M. A similar behavior has been found for Ho-Lu alloys.[46] In contrast, the behavior of Tm is rather surprising [Fig. 5(a)]. c decreases approximately linearly with temperature below T_N at a rate nearly triple that above T_N.

The variations of the magnetic wave vectors with temperature are shown in Fig. 5(b). Our results are in reasonably good agreement with the results of earlier x-ray- and neutron-scattering studies. We will therefore comment only briefly on them. At T_N the values of the wave vectors of Ho, Er, and Tm are clustered near $0.28c^*$, while that of Dy is smaller, $\tau \approx 0.243c^*$. The wave vectors of both Er and Tm increase below T_N until about 0.6 and $0.5T_N$, respectively, where each locks to the value $(\frac{2}{7})c^*$. The spin-flip structures in each case are ferrimagnetic,[20,21,44] with basal-plane and CAM antiferromagnetic components. In Tm, the wave vector remains locked at $(\frac{2}{7})c^*$ for all lower temperatures, while in Er there are several more lock-in transformations, to $(\frac{6}{23})c^*$, $(\frac{1}{4})c^*$, and $(\frac{5}{21})c^*$, at lower temperatures. Still other lock-in transformations observed in earlier studies of Er were not observed in the present experiments as a result of the relatively larger temperature steps taken here. The temperature dependence of the wave vectors of Ho and Dy are also similar to earlier studies. The wave vector of Ho shows an inflection point near $T=0.5T_N$ [with $\tau \approx (\frac{2}{9})c^*$] and a lock-in transformation to $(\frac{1}{6})c^*$ at about $0.13T_N$. At the ferromagnetic transformation in Dy near $0.55T_N$, the wave vector jumps discontinuously to 0. It is intriguing that the first indications of commensurate behavior are manifest in each sample between about 0.5 and $0.6T_N$.

C. Peak widths and magnetic correlation lengths

The temperature dependence of the widths of the primary magnetic satellites measured in scans along the $(0,0,L)$ direction is shown in Fig. 7. The instrumental resolution has not been deconvolved from the data shown in the figure. A minimum in the width of the instrumental resolution for longitudinal scans occurs for wave vectors near $Q=1.8$ Å^{-1}, which happens to be near the position of the $(0,0,2-\tau)$ magnetic satellite in the rare earths.[31] As an approximate indication of the resolution, the FWHM widths of the (002) reflections are $8.5\times10^{-4}c^*$, $1.2\times10^{-3}c^*$, $1.3\times10^{-3}c^*$, and $1.4\times10^{-3}c^*$ for Ho, Er, Dy, and Tm, respectively (see horizontal, dotted lines in Fig. 7).

Between T_N and $0.6T_N$, the longitudinal widths are all

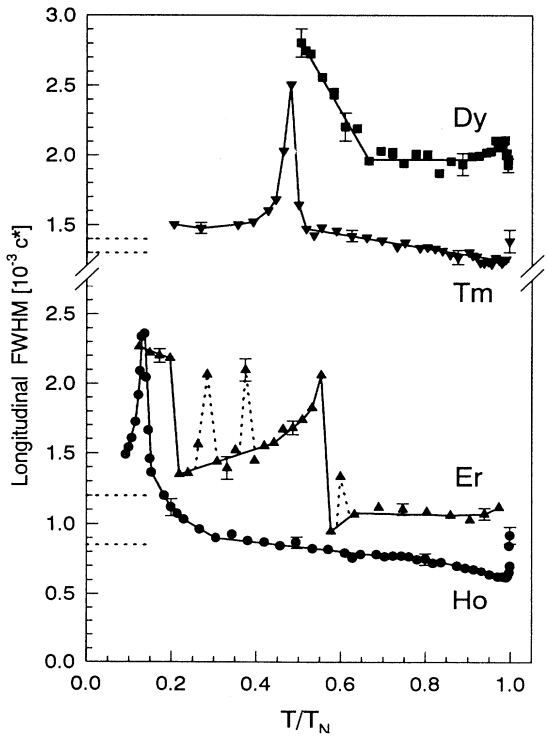

FIG. 7. Longitudinal FWHM vs temperature for the $(0,0,2-\tau)$ magnetic peaks of Dy, Ho, and Tm and the $(0,0,2+\tau)$ peak of Er. (Note the break in the y axis between the Er and the Tm curves.) The solid lines are guides to the eye. The horizontal, dotted lines at the left axis show the widths of the (0,0,2) charge peak for Tm, Dy, Er, and Ho (top to bottom).

approximately constant or increase slightly with decreasing temperature. For the case of Ho, the width of the magnetic peak at $(0,0,2-\tau)$ is resolution limited near T_N and broadens below, as has been discussed elsewhere.[31] This corresponds to a decrease in the magnetic correlation length from more than 5000 Å at T_N (which equals the x-ray penetration depth), to about 1000 Å at $0.13T_N$. The shortest correlation length is observed just above the transition to the conical ferromagnetic phase when $\tau \approx 0.18c^*$. Just below the transition to $\tau=(\frac{1}{6})c^*$, the magnetic peak width decreases again, which presumably reflects the growth of domains in the conical phase.

The longitudinal width of the magnetic peak at $(0,0,2+\tau)$ of Er is nearly resolution limited in the c-axis modulated phase, and reaches its minimum in the $\tau=(\frac{2}{7})c^*$ ferrimagnetic, cycloidal phase below $T=0.6T_N$. The FWHM broadens considerably when the magnetic wave vector decreases below the commensurate value $(\frac{2}{7})c^*$. It decreases again for temperatures below $0.55T_N$, except at 0.37 and $0.28T_N$, where it exhibits sharp excursions over a narrow temperature range. These temperature ranges correspond to the transitions to the commensurate, ferrimagnetic phases with wave vectors equal to $(\frac{4}{15})$ and $(\frac{1}{4})c^*$, respectively, and involve coexistence of commensurate and incommensurate peaks. For the temperatures at which two peaks can be cleanly resolved, the commensurate peak widths are close to the resolution width and the incommensurate peaks are broad. The sharp increases shown with dotted lines in the figure occur prior to each commensurate transition; the subsequent decreases reflect the formation of the commensurate phase. The magnetic peak width of Er increases one last time near $0.2T_N$ at the transition to the conical ferromagnetic phase with wave vector $\tau=(\frac{5}{21})c^*$. In this phase the magnetic peak FWHM reaches its largest value, corresponding to a correlation length of about 1000 Å, and does not decrease. The broadening observed in Tm at $0.5T_N$ is very similar to that observed in Er at $0.6T_N$, the temperatures at which both magnetic structures exhibit transitions from c-axis modulated phases to ferrimagnetic cycloidal phases[47] with $\tau=(\frac{2}{7})c^*$.

For Dy, the longitudinal width of the primary magnetic satellite is broader than the instrumental resolution at all temperatures, corresponding to a maximum correlation length on the order of a few thousand angstroms. The width of the magnetic peak broadens further at about $0.65T_N$, and increases by nearly 30% at the transition to the ferromagnetic phase at $0.5T_N$. It is interesting that in every case the transitions to structures with ferromagnetic components, whether conical spirals, cycloids, or ferromagnets, are apparently preceded by broadening of the magnetic peaks. All of these transitions are first order and, except for Tm, accompanied by significant changes in the c-axis lattice constants as shown in Fig. 5. It seems clear that the broadening signals the loss of long-range magnetic order as a result of the increasing magnetoelastic strain in the lattice, which ultimately leads to the ferrimagnetic and ferromagnetic transitions.

The transverse widths of the primary magnetic satellites (data not shown) are all larger than the experimental resolution and are nearly independent of temperature. For the Ho sample, the width corresponds to in-plane correlation lengths exceeding 6000 Å;[31] for Dy, Er, and Tm it is considerably less ($\sim$1000 Å). These differences are related to the much better crystal mosaic of the Ho sample (see Table I) as compared to the other samples.

IV. CONCLUSIONS

We have performed new measurements of the critical exponents β describing the antiferromagnetic phase transitions of the heavy rare-earth metals using high-resolution x-ray-scattering techniques. It has been possible to obtain critical exponents for secondary order parameters up to order four, derived from the temperature dependence of higher harmonic satellites. Although there are minor differences between our measured critical exponents β for Ho and Dy, they are (to within the error bars) consistent with each other and with the values found earlier from neutron-scattering experiments. The values of β for Er and Tm are different from those of the spiral rare earths. Instead, β and the exponents β_n of the higher harmonics are consistent with mean-field behavior, which was not expected from theoretical arguments. High-resolution measurements of the changes in lattice constants induced by the antiferromagnetic ordering showed a nearly quadratic dependence on sublattice magnetization for Ho and Dy, consistent with the simplest theory. Reduction of the magnetic correlation lengths were observed near all the transitions to ferromagnetic or ferrimagnetic phases with commensurate magnetic wave vectors.

ACKNOWLEDGMENTS

We have benefitted from discussions with J. D. Axe, P. Bak, L. Berman, M. Blume, P. Carra, R. A. Cowley, J. P. Hannon, M. Paczuski, and G. Watson. This work was supported by the U.S. Department of Energy under Contract No. DE-AC02-76CH00016. G. H. acknowledges the Research Council of Norway for financial support.

[1] K. A. McEwen, in *Handbook on the Physics and Chemistry of Rare Earths,* edited by K. A. Cschneider and L. Eyring (North-Holland, Amsterdam, 1978), Vol. 1, p. 411.

[2] J. J. Rhyne, in *Handbook on the Physics and Chemistry of Rare Earths,* edited by K. A. Gschneider and L. Eyring (Elsevier, Amsterdam, 1988), Vol. 11, p. 293.

[3] J. Jensen and A. R. Macintosh, *Rare Earth Magnetism* (Clarendon, Oxford, 1991).

[4] J. Wang, D. P. Belanger, and B. D. Gaulin, Phys. Rev. Lett. **66**, 3195 (1991); B. D. Gaulin, M. Hagen, and H. R. Child, J.

Phys. (Paris) Colloq. **49**, C8-327 (1988).
[5]H. Lin, M. F. Collins, and T. M. Holden, J. Appl. Phys. **73**, 5341 (1993).
[6]M. Hagen, H. R. Child, J. A. Fernandez-Baca, and J. L. Zarestky, J. Phys. Condens. Matter **4**, 8879 (1992).
[7]A. M. Venter, P. V. du Plessis, G. A. Eloff, and E. Fawcett, J. Phys. Condens. Matter **2**, 1363 (1990).
[8]D. A. Tindall, M. O. Steinitz, and M. L. Plumer, J. Phys. F **7**, L263 (1977); M. O. Steinitz, M. Kahrizi, and D. A. Tindall, Phys. Rev. B **36**, 783 (1987).
[9]S. W. Zochowski, D. A. Tindall, M. Kahrizi, J. Genossar, and M. O. Steinitz, J. Magn. Magn. Mater. **54-57**, 707 (1986).
[10]P. Bak and D. Mukamel, Phys. Rev. B **13**, 5086 (1976).
[11]H. Kawamura, J. Appl. Phys. **63**, 3086 (1988).
[12]Z. Barak and M. B. Walker, Phys. Rev. B **25**, 1969 (1982).
[13]P. Azaria, B. Delmotte, and T. Jolicouer, Phys. Rev. Lett. **64**, 3175 (1990).
[14]G. A. Baker, Jr., B. G. Nickel, and D. I. Meiron, Phys. Rev. B **17**, 1365 (1978).
[15]T. R. Thurston, G. Helgesen, D. Gibbs, J. P. Hill, B. D. Gaulin, and G. Shirane, Phys. Rev. Lett. **70**, 3151 (1993); T. R. Thurston, G. Helgesen, J. P. Hill, D. Gibbs, B. D. Gaulin, and P. J. Simpson, Phys. Rev. B **49**, 15 730 (1994).
[16]P. Gehring, K. Hirota, C. F. Majkrzak, and G. Shirane, Phys. Rev. Lett. **71**, 1087 (1993).
[17]S. Langridge, W. G. Stirling, G. H. Lander, J. Rebizant, J. C. Spirlet, D. Gibbs, and O. Vogt, Europhys. Lett. **25**, 137 (1994).
[18]D. Gibbs, G. Grübel, D. R. Harshman, E. D. Isaacs, D. B. McWhan, D. Mills, and C. Vettier, Phys. Rev. Lett. **61**, 1241 (1988).
[19]D. Gibbs, G. Grübel, D. R. Harshman, E. D. Isaacs, D. B. McWhan, D. Mills, and C. Vettier, Phys. Rev. B **43**, 5663 (1991).
[20]D. Gibbs, J. Bohr, J. D. Axe, D. E. Moncton, and K. L. D'Amico, Phys. Rev. B **34**, 8182 (1986).
[21]J. Bohr, D. Gibbs, and K. Huang, Phys. Rev. B **42**, 4322 (1990).
[22]R. A. Cowley and A. D. Bruce, J. Phys. C **11**, 3577 (1978).
[23]A. J. Bevolo, B. J. Beaudry, and K. A. Gschneidner, Jr., J. Electrochem. Soc. **127**, 2556 (1980).
[24]J. P. Hannon, G. T. Trammel, M. Blume, and D. Gibbs, Phys. Rev. Lett. **61**, 1245 (1988).
[25]E. D. Isaacs, D. B. McWhan, C. Peters, G. E. Ice, D. P. Siddons, J. B. Hastings, C. Vettier, and O. Vogt, Phys. Rev. Lett. **62**, 1671 (1989); D. B. McWhan, C. Vettier, E. D. Isaacs, G. E. Ice, D. P. Siddons, J. B. Hastings, C. Peters, and O. Vogt, Phys. Rev. B **42**, 6007 (1990).
[26]M. K. Sanyal, D. Gibbs, J. Bohr, and M. Wulff, Phys. Rev. B **49**, 1079 (1994).
[27]J. P. Hill and D. F. McMorrow (unpublished).
[28]J. Luo, G. T. Trammel, and J. P. Hannon, Phys. Rev. Lett. **71**, 287 (1993).
[29]M. Blume, P. Carra, and J. P. Hannon (private communication).
[30]M. Hamrick, Ph.D. thesis, Rice University, 1994 (unpublished).
[31]G. Helgesen, J. P. Hill, T. R. Thurston, D. Gibbs, J. Kwo, and M. Hong, Phys. Rev. B **50**, 2990 (1994).
[32]K. Iwasa, N. Wakabayashi, T. Takabatake, H. Fujii, and T. Shigeoka, J. Phys. Soc. Jpn. **63**, 127 (1994).
[33]M. Habenschuss, C. Stassis, S. K. Sinha, H. W. Deckman, and F. H. Spedding, Phys. Rev. B **10**, 1020 (1974).
[34]P. de V. du Plessis, C. F. van Doorn, and D. C. van Delden, J. Magn. Magn. Mater. **40**, 91 (1983).
[35]E. Loh, C. L. Chien, and J. C. Walker, Phys. Lett. **49A**, 357 (1974).
[36]J. Eckert and G. Shirane, Solid State Commun. **19**, 911 (1976).
[37]P. de V. du Plessis, G. H. F. Brits, and G. A. Eloff, J. Phys. (Paris) Colloq. **49**, C8-353 (1988).
[38]C. F. Majkrzak, J. D. Axe, and A. D. Bruce, Phys. Rev. B **22**, 5278 (1980).
[39]J. D. Brock, A. Aharony, R. J. Birgeneau, K. W. Evans-Lutterrodt, J. D. Litster, P. M. Horn, G. B. Stephenson, and A. R. Tajbakhsh, Phys. Rev. Lett. **57**, 98 (1986).
[40]A. Aharony, R. J. Birgeneau, J. D. Brock, and J. D. Litster, Phys. Rev. Lett. **57**, 1012 (1986).
[41]B. Fourcade and A.-M. S. Tremblay, Phys. Rev. B **39**, 6819 (1989).
[42]It should be noted that the value of the 2τ exponent for Tm reported here is significantly different from that obtained on the same sample by Bohr, Gibbs, and Huang (Ref. 21). We believe this reflects the lack of data for temperatures very close to T_N in that study, which limits the accuracy in determining T_N.
[43]F. J. Darnell, Phys. Rev. **130**, 1825 (1963).
[44]J. Jensen and R. A. Cowley, Europhys. Lett. **21**, 705 (1993).
[45]J. J. Rhyne and S. Legvold, Phys. Rev. **140**, A2143 (1965).
[46]R. A. Cowley (private communication).
[47]This statement assumes that the $(\frac{2}{7})$ structures of Er and Tm are similar. However, it should be made clear that to our knowledge no analysis of the magnetic structure of Tm in terms of a cycloidal structure has yet been made.